PASJ: Publ. Astron. Soc. Japan **59**, S801–S806, 2007 November 30

Coronal Dimming Observed with Hinode: Outflows Related to a Coronal Mass Ejection

Louise K. HARRA,[1] Hirohisa HARA,[2] Shinsuke IMADA,[2] Peter R. YOUNG,[3] David R. WILLIAMS,[1]
Alphonse C. STERLING,[4*] Clarence KORENDYKE,[5] and Gemma D. R. ATTRILL[1]
[1]*UCL-Mullard Space Science Laboratory, Holmbury St. Mary, Dorking, Surrey, RH5 6NT, UK*
lkh@mssl.ucl.ac.uk
[2]*National Astronomical Observatory of Japan, 2-21-1 Osawa, Mitaka, Tokyo 181-8588*
[3]*STFC, Rutherford Appleton Laboratory, Chilton, Didcot, Oxfordshire OX11 0QX, UK*
[4]*NASA/Marshall Space Flight Center, VP62/Space Science Office, Huntsville, AL 35812, USA*
[5]*Naval Research Laboratory, E.O. Hulburt Centre for Space Research, Washington, DC 20375-5320, USA*

(Received 2007 May 23; accepted 2007 August 14)

Abstract

Coronal dimming has been a signature used to determine the source of plasma that forms part of a coronal mass ejection (CME) for many years. Generally dimming is detected through imaging instruments such as SOHO EIT by taking difference images. Hinode tracked active region 10930 from which there were a series of flares. We combined dimming observations from EIT with Hinode data to show the impact of flares and coronal mass ejections on the region surrounding the flaring active region, and we discuss evidence that the eruption resulted in a prolonged steady outflow of material from the corona. The dimming region shows clear structure with extended loops whose footpoints are the source of the strongest outflow ($\approx$ 40 km s^{-1}). This confirms that the loops that are disrupted during the event do lose plasma and hence are likely to form part of the CME. This is the first time the velocity of the coronal plasma has been measured in an extended dimming region away from the flare core. In addition there was a weaker steady outflow from extended, faint loops outside the active region before the eruption, which is also long lasting. These were disturbed and the velocity increased following the flare. Such outflows could be the source of the slow solar wind.

Key words: Sun: activity — Sun: coronal mass ejections — Sun: flares — Sun: UV radiation

1. Introduction

Understanding the source of coronal mass ejections (CMEs) has implications for the understanding of the Sun–Earth system. In order to track a CME from the Sun to the Earth it is important to understand the actual source region. This can be difficult since CMEs are best seen in coronagraph data in which the solar disk is obscured. However signatures have been studied over the years that are summarized in Hudson and Cliver (2001). Coronal "dimming" is one of the main on-disk signatures of a CME. When originally discovered during the Skylab era they were called "transient coronal holes" (e.g., Rust 1983). Coronal dimming characteristics suggest they are due to a loss of coronal plasma. Sterling and Hudson (1997) showed a very clear example of dimming using data from the Soft X-ray Telescope on Yohkoh. These dimmings persisted for three days following the flare and related halo CME. In this case it was suggested that the dimmings were consistent with the source of the CME being a flux rope that erupted leaving behind the dimming regions. Similar behaviour has also been observed in SOHO-Extreme ultraviolet Imaging Telescope (EIT) data (e.g., Thompson et al. 1998). Estimates have also been made of how much mass the dimming regions could contribute to the CME — these have been found to be $\geq$ 50% of the total mass of the CME (e.g., Zhukov & Auchère 2004; Sterling & Hudson 1997; Harrison & Lyons 2000). Attrill et al. (2006) and Crooker and Webb (2006) studied the simple case of the 1997 May 12 event and found that although there were two dimming regions, consistent with the idea of an erupting flux rope, the northern-most dimming region underwent interchange reconnection with the north polar coronal hole which changed the region's magnetic connectivity so that the flux rope only remained anchored to the Sun at the southern-most dimming region. That example demonstrated that even in the simplest case, occuring at a quiet time on the Sun, large-scale magnetic interactions are always possible that can confuse our understanding of the magnetic structure of the subsequent interplanetary CME. In order to make sense of the source region of a CME we need to understand the physical structure of the dimming regions and how these evolve and expand across the disk.

Quantitative measurements of dimming regions are inherently difficult since the emission is weak in these regions. Measurements such as the time variation and mass content have been determined from imaging data. Spectroscopic measurements of velocities have been difficult due to temporal and spectral resolution limitations so far. Harra and Sterling (2001) found two examples of Doppler velocity measurements from SOHO-CDS — the first was on the limb and showed velocities in the erupting region of 30 km s^{-1}. The second was in a dimming region that followed a coronal wave. Velocity

* Current address: Institute of Space and Astronautical Science, JAXA, Hinode Group, 3-1-1 Yoshinodai, Sagamihara, Kanagawa 229-8510.

measurements could only be made in the transition region at this location due to the weak coronal emission. In order to understand the physical processes within a dimming region which are so closely tied to the behaviour of CMEs, we must understand the structure (both coronal and magnetic) of the dimming region along with the velocity information.

In this paper, we study an active region that is flare productive — NOAA AR 10930. This region began to rotate into view on 2006 December 5. We concentrate mostly on the large GOES X-class flare that was produced on 2006 December 14. This flare was related to a coronal mass ejection, a "coronal EIT wave", and had a large dimming region associated with it. The Hinode mission observed this flare, and in particular the EUV Imaging Spectrometer (EIS) was pointed at the dimming region. This allowed us to measure for the first time the Doppler velocities in the dimming regions outside the flare core site where the coronal emission is weak. Hinode EIS has the dynamic range and spectral resolution to measure this.

2. Instrumentation

2.1. Hinode

The Hinode space mission (Kosugi et al. 2007) was launched on 2006 September 22 at 21:36 UT. It is a Japanese–US–UK mission and includes three instruments on board: the Solar Optical Telescope (SOT), the X-Ray Telescope (XRT), and the EUV Imaging Spectrometer (EIS). This paper will concentrate on datasets from EIS. The EIS instrument (Culhane et al. 2007) has 2 wavebands: 166–211 Å and 246–292 Å. It has 4 slit/slot positions: 1″, 2″, 40″, and 266″, allowing a wide choice of modes of operation. In this paper we will concentrate on data taken with the 1″ slit and using the fine mirror movement to "raster" and build up an image. For the dataset on December 14, there was a 1″ raster with 256 steps and a height of 256″. The spectral resolution is 0.0223 Å per pixel, which corresponds to a Doppler velocity resolution of 2 km s^{-1} for reasonable statistics. The pixel size is 1″.

We calibrated the EIS data using the eis_prep routine in the SolarSoft software package (Freeland & Handy 1998), which corrects for flat field, dark current, cosmic rays, hot pixels, wavelength, and absolute calibration. In addition, one of the instrumental effects that needs to be removed is the orbital variation of the line position. This is caused by thermal effects on the instrument and it follows a sinusoidal behavior. This was removed by modelling the effect in the region at the south part of the raster, away from the active region emission.

2.2. SOHO

For context images we made use of the Extreme ultraviolet Imaging Telescope (EIT) on SOHO (Delaboudinière et al. 1995). We used the EIT images in the 195 Å filter. The EIT data have a cadence of 12 min and a pixel size of 2.″6 pixels. We used base difference images for our analysis, which required that differential rotation be taken into consideration before subtraction.

3. The Flare and Coronal Mass Ejection

The flare that we concentrate on occurred on December 14 beginning just before 22:00 UT. The X-ray level peaked less than 30 min later with a GOES X-class flare, and returned to the background level by approximately 06:00 UT the next day. Figure 1 shows the GOES X-ray lightcurve in the 1–8 Å band with the EIS observation mode over-plotted. Before the flare began EIS carried out a 1″ raster. During the flare rise it switches to the 40″ slot and in the flare decay it returns to the 1″ raster mode. We will concentrate on the periods when EIS is rastering in order to determine any mass outflows that could be related to the CME.

The CME was described in the LASCO preliminary CME list as an asymmetric halo event with a speed ranging between 970 km s^{-1} and 1220 km s^{-1}. There was a "coronal EIT wave" associated with the CME as reported for some events (see Biesecker et al. 2002).

An EIT base difference image using the 195 Å filter is shown in figure 2. A pre-flare image was subtracted from the image at 01:14 UT. There is a bright region showing the flare site, and to the east there is a deep dark dimming region. In this region the intensity drops by more than 60% of its original intensity reaching close to the quiet Sun level. However, the intensity does not become as low as the coronal hole intensity. This is seen clearly in figure 3 and is similar to that observed by Attrill et al. (2006).

Figure 4 shows the EUV intensity images around the time of the flare. The dramatic changes in the magnetic structures are clearly seen.

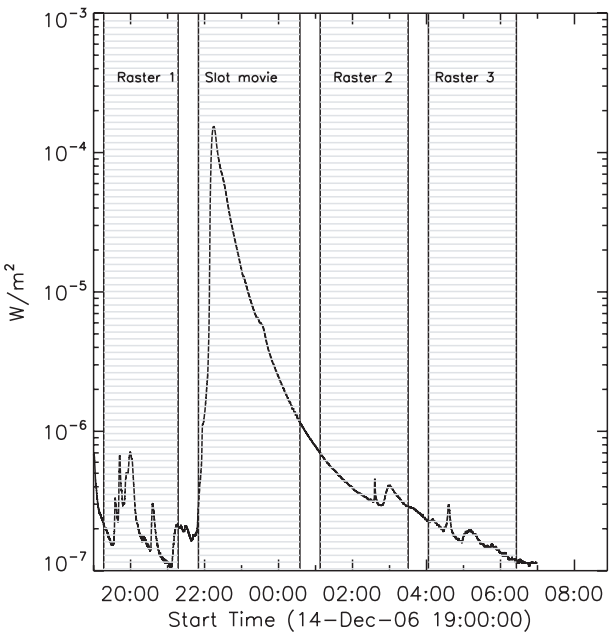

Fig. 1. GOES low energy channel lightcurve with the time periods of the EIS rasters and slot movies highlighted.

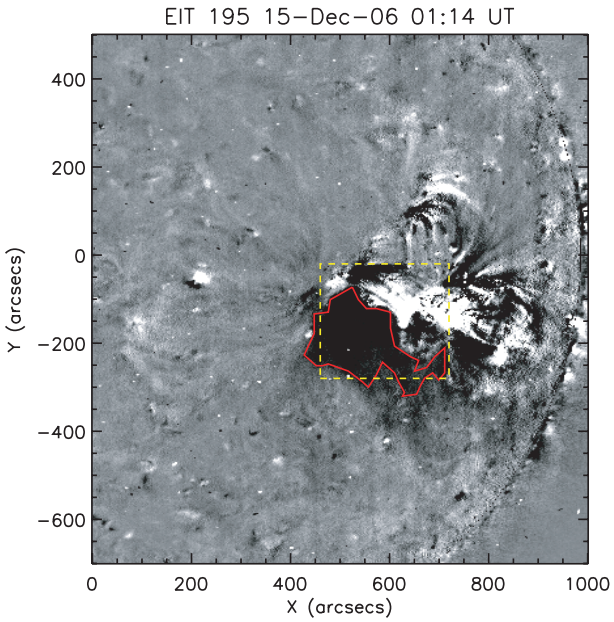

Fig. 2. EIT base difference image with the preflare image at December 14, 21:12 UT subtracted from the image on December 15, 01:14 UT. The EIS field of view is shown by a yellow dashed line. The red contour is the dimming negion.

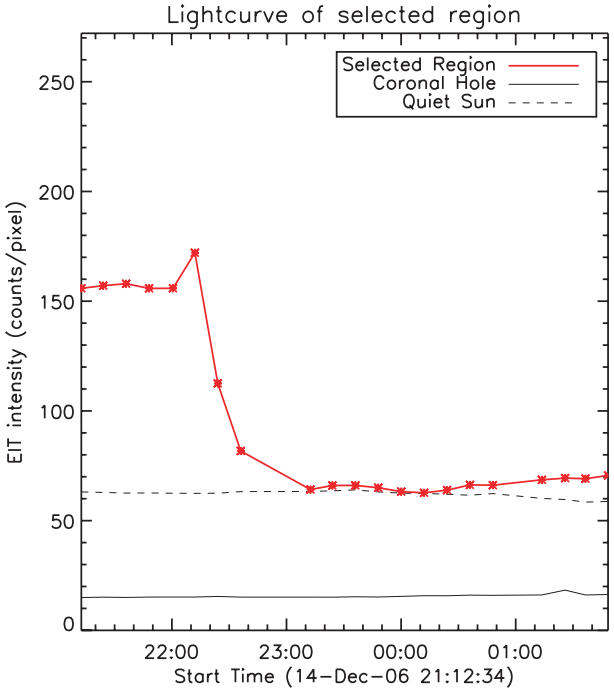

Fig. 3. Light curve of the dimming region marked by the red contour seen in figure 2 from EIT data. There is a sudden decrease of intensity which drops to close to the quiet Sun intensity level (marked with a dashed line). The solid line shows the coronal hole intensity level.

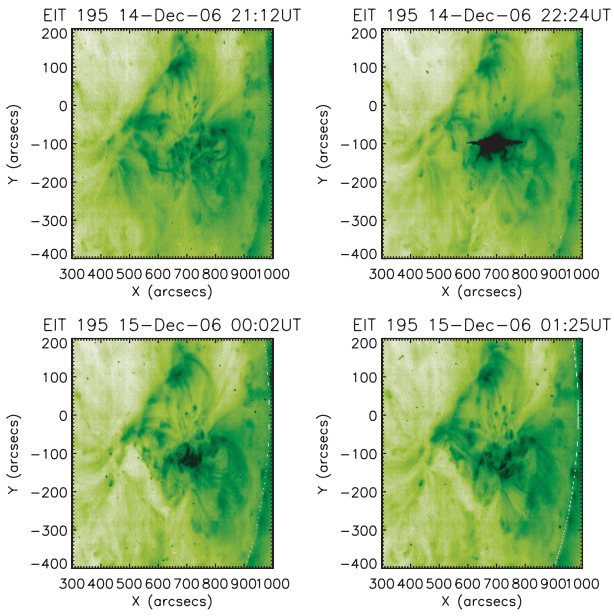

Fig. 4. EIT reverse intensity images showing the evolution of the flare and the surrounding region. The dimming region can be clearly seen as the long faint loops are disrupted following the flare (cf. figure 2). The intensity maps are in log scale to show the weaker intensity regions that are related to the outflowing material.

4. Coronal Dimming: Velocity Measurements

Previously it has been very difficult to measure outflowing velocities related to coronal dimming. This is due to the fact that by its nature the emission is weak. The EIS instrument has the sensitivity and the spectral resolution to measure the flows in such dimming regions accurately. We concentrate on the strongest lines in this EIS study: Fe X 184.5 Å, Fe XII 195.12 Å, He II 265.32 Å, Fe XIV 274.2 Å, Fe XV 284.16 Å, where the wavelength given is the centre of the EIS spectral window. Each spectral window is 24 pixels wide, with each pixel being equivalent to 25 km s^{-1}. For each pixel position we fitted a Gaussian profile to each spectral window in order to determine the Doppler shift. The "rest" position was taken to be the average of the whole raster scan, so the velocities obtained are relative velocities. Corrections were made as described in the previous section.

Figure 5 shows the intensity and Doppler velocity maps for Fe XV before the flare started and in the decay phase of the flare. The flare core is at the west edge of the images (right-hand side) so the EIS field of view encompasses the weaker emission away from the core site. Before the flare begins, flows are seen in the active region, and in particular at the edges an outflow (blue shift) is seen. This seems to be related to large-scale, faint loop structures at the edge of the active region. Following the flare dramatic changes can be seen in the structure with a sharp reduction in coronal emission observed (i.e., dimming locations). In addition the outflows increase with red-shifts (down flows) being seen around the main post-flare loops. This is expected in the decay phase of flares when the plasma cools. More interestingly there are strong blue shifts seen at the region where the above-mentioned coronal dimming occurs.

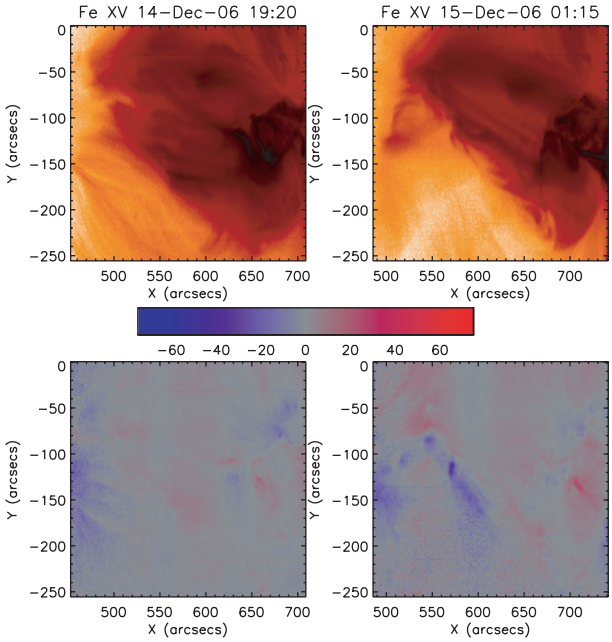

Fig. 5. EIS Fe XV reverse intensity map showing the raster before the flare began and after the peak of the flare. There is a clear reduction in coronal material. The intensity maps are in log scale to show the weaker intensity regions that are related to the outflowing material. The velocity maps at each time are shown below. There is outflowing (blue) material in the core of the coronal dimming region. The colour bar shows the velocity scale which is in km s^{-1}.

The outflow is structured with higher velocities seen at what appears to be footpoint locations, and also being seen along long loop-like structures.

In figure 6, the same plots of intensity map and velocity maps are shown for a range of ions. These confirm that dimming is seen across a range of temperatures in the corona (1–2 MK). There is also evidence of blue-shift in the dimming regions seen in the He II band. The velocity structure is different to the coronal lines with the blue-shift also in the centre of the dimming region. Dimmings have been seen at such low temperatures before (e.g., Jiang et al. 2006).

The EIS Fe XII difference image is shown in figure 7 (bottom). The blue-shifted Doppler velocities are overlaid on the difference image and found to be within the very core of the deep dimming region. The strongest outflowing material is from regions of weak positive magnetic polarity as seen in the MDI image (figure 7, top left). The regions were related to loops in the pre-event configuration. The EIS difference image shows that the loops have reduced in intensity significantly, and some of the loops may have erupted. It is most likely that it is a density drop rather than a temperature change since the dimming is seen in a range of different temperature Fe lines. In addition the strongest outflows are at the footpoints of the loops that have strong dimming, indicating continuous outflow. These velocities peak around 40 km s^{-1}. Along the loops the velocities peak at $\approx$ 20 km s^{-1}. The velocities are long-lasting, and are also seen in raster 3 labelled in figure 1. This is towards the end of the flare, and the dimming region has not returned to its pre-eruption coronal level, so we may yet still expect

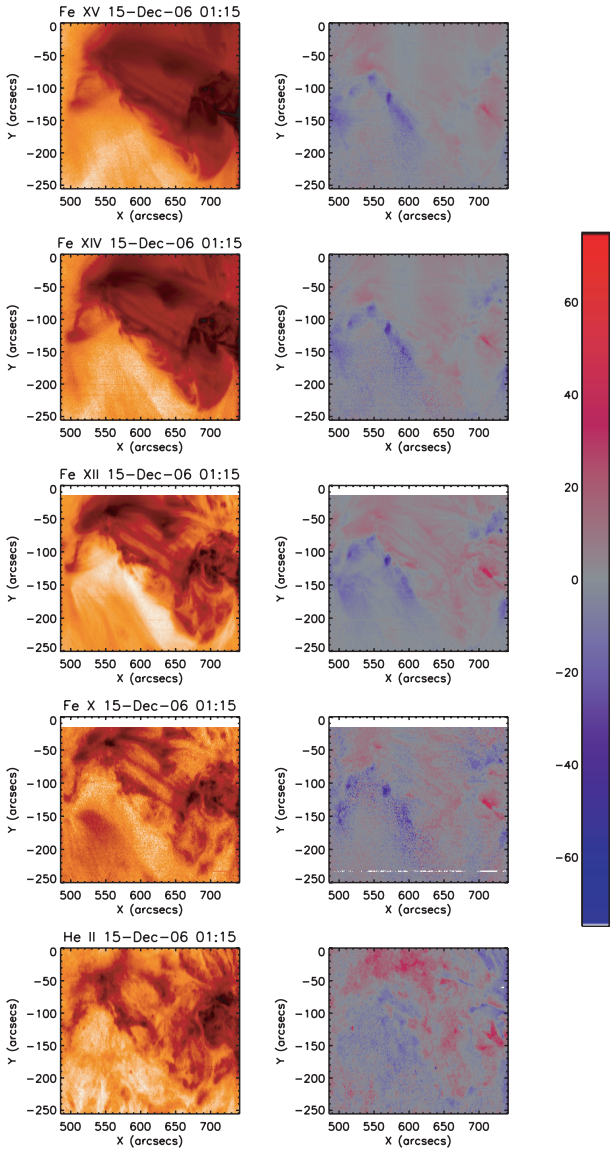

Fig. 6. EIS intensity and velocity maps for a range of ions [Fe XV (log T = 6.3), Fe XIV (log T = 6.3), Fe XII (log T = 6.1), Fe X (log T = 6.0), He II (log T = 4.7)] at a time during the decay phase of the flare. The coronal dimming region shows outflow for across these different temperatures. In addition there is evidence for outflow across the different temperature plasmas. The color bar shows the velocity scale which is in km s^{-1}.

outflows to continue. We determined a very rough estimate of mass flux. The intensity in the dimming region determined from Fe XII in EIS dropped to 30% of its value following the flare. We assumed the area involved to be the dimming area seen in the EIS field of view and assumed the average speed to be 20 km s^{-1}. This gives a mass flux of $\approx 2.5 \times 10^{11}$ g s^{-1}.

5. Discussion

Coronal dimming is well known to be related to CMEs. Until now dimming has predominantly been measured through imaging data. Hinode-EIS has allowed a more detailed insight with its combination of high spatial resolution and high spectral

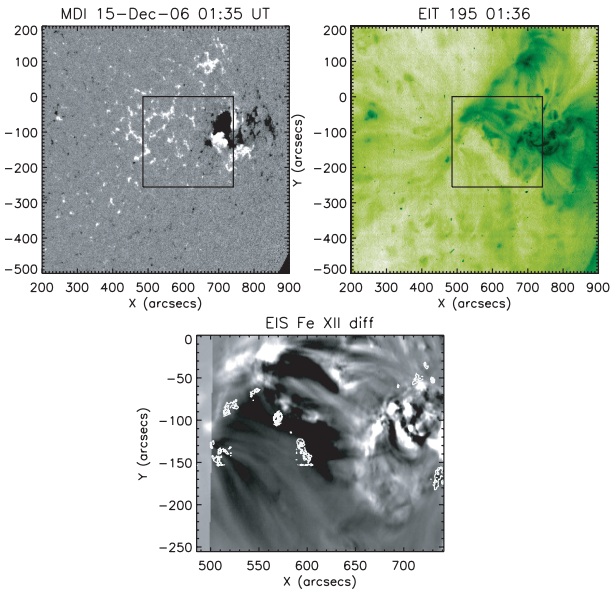

Fig. 7. On the left the magnetogram from MDI is shown with a box illustrating the EIS field of view. On the right the EIT image is shown for context again with a box showing the EIS field of view. The strongest velocities are seen in weak positive polarities in the strong dimming region. The EIS Fe XII intensity difference image with the Doppler velocity contours (blue-shift only) overlaid in white is shown at the bottom. The contour levels range from −10—−50 km s^{-1}.

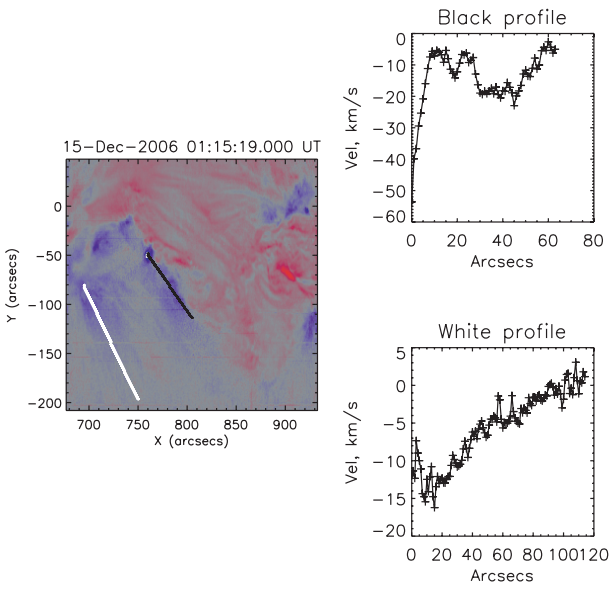

Fig. 8. Velocity map of the Fe XV ion on December 15 shown with 2 lines (black and white) on the left-hand side. The velocity profiles are shown on the right-hand side. The black profile shows variation along the length that demonstrates complexity in the structure. The white profile shows a gradual reduction in the magnitude of the velocity towards the end of the loop suggesting a low-lying structure. For both profiles "0" arcsecs begin on the top.

resolution. Spectroscopy with Hinode-EIS has now, for the first time, allowed an accurate velocity field in the corona to be measured for a dimming region: the high sensitivity of the instrument enabling emission line profiles to be accurately measured in areas of low intensity, while still retaining the high instrument spatial resolution. We could not measure such coronal emission with previous spectrometers. We observed the deep dimming region that was seen in a range of different temperature plasma from He II at $\approx 10^4$ K to Fe XV at 2 MK. The highest velocities measured appear to be at the footpoints of extended, faint loops away from the flare core site. Rather than seeing merely amorphous "regions" of dimming we can now observe that the dimming region is structured, with the deepest core region being at the footpoints of loops. Being able to observe the corona in velocity space allows us to confirm that the dimming regions are locations of outflowing plasma.

Large-scale disruption from flares and CMEs has been observed before. Remote brightenings have been found above the region where dimming was subsequently formed (e.g., Manoharan et al. 1996). Liu et al. (2006) also found remote brightenings seen in Hα data and concluded that these regions were magnetically connected to the flaring active region. The remote brightenings were due to an erupting flux rope interacting with the overlying magnetic field.

In addition we observed Doppler signatures consistent with outflow from very weak extended loops before the flare began. Indeed this outflow was observed in the same active region two days beforehand on December 12. At this stage the active region was not flaring significantly — the first X-class flare did not occur until December 13. A number of C-class flares had occurred on December 11. Following the large flare on December 13 the outflow in the same region increased to over 100 km s^{-1}. The latter is described in Imada et al. (2007).

For the first time we have been able to measure the structure of the outflow. We observed the highest outflow at what appears to be the footpoints of long structures (≈ 60 km s^{-1}), and along those loop structures we measured velocities of ≈ 20 km s^{-1}. Velocity profiles along two such structures are shown in figure 8. The profile furthest away from the flaring site (figure 8, white profile) shows a relatively smooth decrease in velocity from the high velocity region to lowest suggesting a continuous structure that is low-lying. The blue-shifted structure closest to the flaring region (figure 8, black profile) shows a fluctuating structure suggesting complexity. In both cases the blue shifted region are clearly showing a reduction in intensity (see figure 5). In order to understand these structures further we would need a detailed understanding of the magnetic field before and after the eruption. It is difficult to rule out absolutely that these flows are not due to flows along loop rather than true outflows. Nonetheless we did not observe a redshift at the end of the loops which would be consistent with loop flows; this supports that our observations represent true outflows. Future studies will clarify this question.

What is also interesting is that before the flare occurs there is also much weaker outflow to the east of the active region. It is not clear whether this was outflowing plasma from a previous eruption, or a steady outflow that is always there. Long lasting outflows such as these are likely to contribute to the slow solar wind.

There has been much progress in CME modelling in recent years (e.g., Forbes 2000) — however there is still a lack of understanding of the coupling between the small scales that we

are observing and the large scales seen in coronagraph data. In the future we intend to analyse the magnetic field in more detail in order to determine if we are viewing open or closed magnetic fields. What we are seeing could be a magnetic reconfiguration following the flare that causes reconnection with other field lines elsewhere. Or indeed what we are observing could be similar to the "coronal funnels" seen in coronal holes by Tu et al. (2005). In their case the plasma is accelerated in a funnel above 5 Mm, but originates from small loops below.

Hinode is a Japanese mission developed and launched by ISAS/JAXA, with NAOJ as domestic partner and NASA and STFC (UK) as international partners. It is operated by these agencies in co-operation with ESA and NSC (Norway).

References

Attrill, G., Nakwacki, M. S., Harra, L. K., van Driel-Gesztelyi, L., Mandrini, C. H., Dasso, S., & Wang, J. 2006, Solar Phys., 238, 117

Biesecker, D. A., Myers, D. C., Thompson, B. J., Hammer, D. M., & Vourlidas, A. 2002, ApJ, 569, 1009

Crooker, N. U., & Webb, D. F. 2006, JGR, 111, A08108

Culhane, J. L., et al. 2007, Solar Phys., 243, 19

Delaboudinière, J. -P., et al. 1995, Solar Phys., 162, 291

Forbes, T. G. 2000, JGR, 105, 23153

Freeland, S. L., & Handy, B. N. 1998, Solar Phys., 182, 497

Harra, L. K., & Sterling, A. C. 2001, ApJ, 561, L215

Harrison, R. A., & Lyons, M. 2000, A&A, 358, 1097

Hudson, H. S., & Cliver, E. W. 2001, JGR, 106, A11, 25199

Imada, S., Hara, H., Watanabe, T., Asai, A., Kamio, S., Matsuzaki, K., Harra, L. K., & Mariska, J. T. 2007, PASJ, 59, S793

Jiang, Y.-C., Li, L.-P., & Yang, L.-H. 2006, Chin. J. Astron. Astrophys., 6, 345

Kosugi, T., et al. 2007, Solar Phys., 243, 3

Liu, C., Lee, J., Deng, N., Gary, D. E., & Wang, H. 2006, ApJ, 642, 1205

Manoharan, P. K., van Driel-Gesztelyi, L., Pick, M., & Démoulin, P. 1996, ApJ, 468, L73

Rust, D. M. 1983, Space Sci. Rev., 34, 21

Sterling, A. C., & Hudson, H. S. 1997, ApJ, 491, L55

Thompson, B. J., Plunkett, S. P., Gurman, J. B., Newmark, J. S., St. Cyr, O. C., Michels, D. J., & Delaboudinière, J.-P. 1998, GRL, 25, 2461

Tu, C.-Y., Zhou, C., Marsch, E., Xia, L.-D., Zhao, L., Wang, J.-X., & Wilhelm, K. 2005, Science, 308, 519

Zhukov, A. N., & Auchère, F. 2004 , A&A, 427, 705